Finite-Size Scaling at the Edge of Disorder in a Time-Delay Vicsek Model

Viktor Holubec,[1,2,*] Daniel Geiss,[1,3] Sarah A. M. Loos,[1,5] Klaus Kroy,[1] and Frank Cichos[4]
[1]Institut für Theoretische Physik, Universität Leipzig, Postfach 100 920, D-04009 Leipzig, Germany
[2]Charles University, Faculty of Mathematics and Physics, Department of Macromolecular Physics, V Holešovičkách 2, CZ-180 00 Praha, Czech Republic
[3]Max Planck Institute for Mathematics in the Sciences, D-04103 Leipzig, Germany
[4]Peter Debye Institute for Soft Matter Physics, Universität Leipzig, 04103 Leipzig, Germany
[5]ICTP — International Centre for Theoretical Physics, Strada Costiera 11, 34151, Trieste, Italy

(Received 13 July 2021; revised 29 September 2021; accepted 16 November 2021; published 14 December 2021)

Living many-body systems often exhibit scale-free collective behavior reminiscent of thermal critical phenomena. But their mutual interactions are inevitably retarded due to information processing and delayed actuation. We numerically investigate the consequences for the finite-size scaling in the Vicsek model of motile active matter. A growing delay time initially facilitates but ultimately impedes collective ordering and turns the dynamical scaling from diffusive to ballistic. It provides an alternative explanation of swarm traits previously attributed to inertia.

DOI: 10.1103/PhysRevLett.127.258001

Interacting assemblies of active elements ranging from neural networks in the brain to forest fires and bird flocks can exhibit scale-free behavior [1–4]. This might be indicative of an underlying powerful physical ordering principle overwriting their inherent complexity. Finite-size scaling theory [5] associates such behavior with a correlation length exceeding the system size and conjectured to arise from a mechanism called self-organized criticality [6]. It is indeed an appealing idea that simple interaction rules, when, e.g., individuals replicate actions of their neighbors, can drive a nonequilibrium ensemble toward criticality. Even though it does not generally seem to apply to both natural systems [7,8] and their models [9–11], studying the emergent finite-size scaling in natural assemblies is vital for their prospective modeling in the spirit of nonequilibrium many-body systems, as successful models should be required to reproduce the observed scaling [10] and correlations [12]. In this vein, the inertia spin model [12] was proposed to overcome known deficiencies of the classical Vicsek model (VM) [13] in comparison with empirical data for natural swarms and flocks. Inspired by observations of birds and insects [4], which cannot turn instantaneously, it adds inertia to the navigation rules for the individual motile spins and predicts dynamical scaling with exponent $z = 1.5$ for a small-particle-velocity ("underdamped equilibrium") regime and $z = 1.3$ for a large-velocity ("underdamped off-equilibrium") regime [14]. This brings the VM, with classical exponents $z = 2$ and $z = 1.7$, respectively, closer to the dynamical scaling and time-correlation functions found in natural swarms of moderate size (dynamical exponent $z \approx 1.1$) [15,16].

However, for motile ensembles, physical inertia can have quite similar effects as delayed reactions due to finite speeds of information transfer processing, and actuation [17–19]. Such traits are indeed ubiquitously found in nature, from insects to birds, in various robotic systems [20–22] and are also thought to cause traffic jams [23]. Recent experiments [24,25] with feedback-driven artificial microswimmers [26] have moreover established their role in the naturally overdamped microscopic world of active Brownian particles such as bacteria, for which inertial effects are negligible. Beyond oscillatory behavior, which is also a common trait of inertial motion, time-delayed interactions can give rise to multistability, instabilities, and even chaos [19,27–29]. Conversely, intermediate time delays may facilitate clustering compared with the classical VM [28] and flocking in the Cucker–Smale model [30]. And recent indications that delay-dependent optimizations play a role in artificial microswimmer assemblies [25] seem reminiscent of the optimum run-and-tumble times of bacteria [31,32] or the improved localization achieved with feedback cooling [33,34] or feedback-driving of robots [35].

In this Letter, we demonstrate that the classical VM [13] with retarded reactions exhibits the same finite-size scaling and time correlations near the ordering transition as the inertia spin model [4]. This suggests that scaling and correlations similar to natural swarms can be expected for a wealth of systems with time-delayed interactions, including overdamped Brownian particle assemblies. We can also corroborate the observation that increasing delay times may have a nonmonotonic effect on the stability of coherent collective motion [28].

Model.—The (classical) VM [13] arguably is the simplest model for motile active-particle assemblies, ranging from bacteria to birds, and a central paradigm in the field of motile active matter [36–39]. In each discrete time step, all particles advance with the same constant speed v_0. And they instantaneously adapt their orientations to the previous

average orientation of their neighbors within an interaction sphere of radius R, up to some random error contributed by a local noise term. The orientation is thus clearly an overdamped variable, as it bears no inertia.

In the delay VM, depicted in Fig. S1 of the Supplemental Material [40], particle i adapts at time t to the mean orientation of all particles that had distance less than R from its previous position, at time $t-1-\tau$, with an integer-valued time delay $\tau \geq 0$. The discrete time step and the interaction radius $R=1$ serve as units of time and length, respectively. The dynamics of the standard VM is recovered for $\tau = 0$. The velocity $\mathbf{v}_i$ and position $\mathbf{r}_i$ of particle i in three spatial dimensions (3D) thus obey the set of equations [13]

$$\mathbf{v}_i(t+1) = v_0 \mathcal{R}_\alpha \Theta\left[\mathbf{v}_i(t) + \sum_j n_{ij}(t-\tau)\mathbf{v}_j(t-\tau)\right], \quad (1)$$

$$\mathbf{r}_i(t+1) = \mathbf{r}_i(t) + \mathbf{v}_i(t+1). \quad (2)$$

The noise operator $\mathcal{R}_\alpha X$ randomly rotates its argument X within a uniformly distributed solid angle $4\pi\alpha$ centered around X, and $\Theta(\mathbf{v}) \equiv \mathbf{v}/|\mathbf{v}|$ normalizes its argument. We assume geometric interactions corresponding to the connectivity matrix elements $n_{ij}(t) = 1$ for $i \neq j$ if $r_{ij}(t) = |\mathbf{r}_i(t) - \mathbf{r}_j(t)| < R$, and $n_{ij}(t) = 0$ otherwise.

We simulated the delay VM with fixed speed $v_0 = 0.05$ and noise strength $\alpha = 0.45$ inside a cube with size L^3 and periodic boundary conditions for six values of the particle number $N = 2^n$, $n = 6, \ldots, 11$. In this setting, we repeated the analysis performed in Refs. [15,49] for the static and dynamic scaling and the correlation functions of the standard VM, operating in its overdamped equilibrium regime [14], for delay times $\tau = 0, \ldots, 20$. As control parameter, we prescribed the average nearest-neighbor distance r_1 between the individual particles by varying L. Here, we present the main simulation results. Further data, technical details, and some analytical discussion can be found in the Supplemental Material [40].

The central object for our data analysis is the Fourier transformed spatiotemporal correlation function (CF)

$$C(k,t) = \left\langle \frac{1}{N}\sum_{i,j}^{N} \frac{\sin[k r_{ij}(t,t_0)]}{k r_{ij}(t,t_0)} \delta\hat{\mathbf{v}}_i(t_0)\cdot\delta\hat{\mathbf{v}}_j(t_0+t) \right\rangle \quad (3)$$

of the normalized velocity fluctuations [4,15,40]

$$\delta\hat{\mathbf{v}}_i = \frac{\delta\mathbf{v}_i}{\sqrt{N^{-1}\sum_k \delta\mathbf{v}_k\cdot\delta\mathbf{v}_k}}, \quad (4)$$

where $\delta\mathbf{v}_i = \mathbf{v}_i - \sum_k \mathbf{v}_k/N$ is the deviation of the velocity of particle i from the average velocity, and $r_{ij}(t_0,t) = |\mathbf{r}_i(t_0) - \mathbf{r}_j(t)|$ is the distance between particles i and j at times t and $t_0 < t$. The average $\langle\ldots\rangle$ is taken over t_0 [40].

Static scaling.—At $t = 0$, $C(k,0)$ exhibits a global maximum at $k = k^\star \sim 1/\xi$, where ξ corresponds to the correlation length. Assuming proportionality between fluctuation and response, this value of the CF is interpreted as a susceptibility $\chi \equiv C(k^*,0)$ [4,15,40].

For given delay time τ and particle number N, the susceptibility χ exhibits a maximum $\chi^* = \chi^*(\tau,N)$ as a function of the nearest-neighbour distance at $r_1^* = r_1^*(\tau,N)$. The system is found to be ordered (large average velocity) for $r_1 < r_1^*$ and disordered (small average velocity) otherwise. For a given N, the susceptibility χ^* at the transition decreases monotonically with growing τ and eventually saturates [see Figs. 1(a) and 1(b) and, in the Supplemental Material, Figs. S2 and S3 [40]]. The equal-time orientation correlations are thus generally reduced for retarded as opposed to instantaneous interactions, which suggests that the sensitivity to external perturbations decreases accordingly. For sufficiently large τ and N, the derivative of the susceptibility with respect to r_1 abruptly increases at some $r_1 < r_1^*$; see the vertical dotted line at $r_1 \approx 0.4$ in Fig. 1(b). No such kink is observed for small τ [40]. For a given τ and large enough N, the susceptibility in the vicinity of the ordering transition [49] exhibits finite-size scaling according to Ref. [50]:

$$r_1^* \sim r_C + N^{-1/(3\nu)}, \quad (5)$$

$$\chi \sim N^{\gamma/(3\nu)}. \quad (6)$$

In other words, for any given τ, the limiting location $r_C = r_1^*(\tau,\infty)$ of the transition for large (infinite) particle numbers and the critical exponents γ and ν of the susceptibility $\chi \sim (r_1^* - r_C)^{-\gamma}$ and the correlation length $\xi \sim (r_1^* - r_C)^{-\nu}$, respectively, can all be extrapolated from a data collapse of the susceptibilities for different N. The procedure is illustrated in Figs. 1(c) and 1(d). The resulting exponents and r_C exhibit strong dependencies on τ, which saturate as $\tau v_0/R \approx 1/2$, when the advance during one delay time becomes comparable to the interaction radius [Figs. 1(e)–1(h)]. An analytical argument corroborates that a further increase of τ should not significantly alter the qualitative physical picture [40]. For a particle of characteristic size 2.5 mm traveling with velocity 1 meter per second with an interaction radius of 4× body length (10 mm), the condition $\tau v_0/R = 1/2$ implies a time delay of 5 ms, which are numbers roughly in accord with data available for fruit flies [51–54].

Since the static critical exponents in the standard VM are known to depend strongly on the density, speed, and interaction radius [56], their absolute values are of limited interest. Rather, their trends and dependencies are revealing. The critical nearest-neighbor distance r_C in Fig. 1(h), proportional to the critical density of the system, exhibits a pronounced maximum at $\tau v_0/R \approx 0.2$, indicating that a system with an intermediate delay time favors order already at lower densities as compared with the system without delay. This somewhat counterintuitive result is in agreement with findings of Refs. [28,35] that intermediate delays stabilize collective motion. For larger delay times,

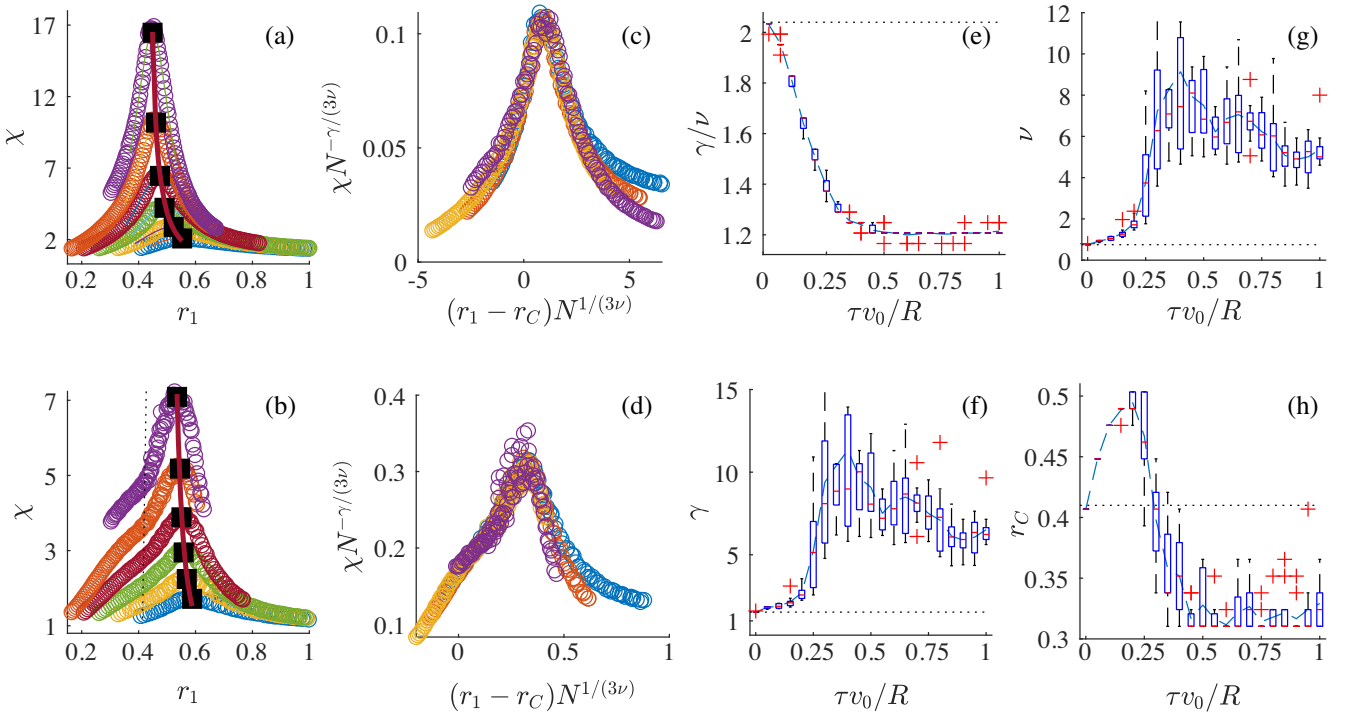

FIG. 1. Static finite-size scaling in the 3D delay VM. Each simulation departed from a random initial state and was evolved for a transient period of 1500 time steps before measurements started. (a),(b) The susceptibilities $\chi \equiv \max_k C(k,0)$ averaged over 11 trajectories of 10^4 time steps for $N = 64, 128, 256, 512, 1024, 2048$ particles (from bottom to top) and delay times $\tau = 0$ [(a), standard VM] and $\tau = 15$ [(b), $\tau v_0/R = 0.75$], respectively, over the mean nearest-neighbour distance r_1. (c),(d) The data collapse achieved for $N \geq 256$. (e)–(h) Box plots [55] of the exponent ratio γ/ν, the individual exponents, and the extrapolated critical parameter r_C for $N \to \infty$, respectively, all for delay times τ from 0 to 20. Broken dashed lines mark averages over the 11 realizations. The horizontal dotted lines depict the values $\nu \approx 0.75$, $\gamma \approx 1.53$, and $r_C \approx 0.41$ obtained for $\tau = 0$, where the model reduces to the standard VM, consistent with the data in Ref. [49]. In (a) and (b), black squares mark susceptibility maxima $\chi(r_1^*)$ and solid lines are computed using the finite-size scaling relation $\chi \sim (r_1^* - r_C)^{-\gamma}$ with parameters from (e)–(h). The vertical dotted line in (b) marks the abrupt changes in the slope of χ.

the critical nearest-neighbor distance r_C drops sharply to a value below that for the standard VM. A possible explanation can be based on the decrease of the maximum susceptibility with delay time, shown in Sec. S2 in the Supplemental Material [40]. The susceptibility measures both the sensitivity to destabilizing perturbations and the ability to align in the flocking regime. The local maximum in r_C could thus originate from a trade-off between these tendencies, the increased resistance to fluctuations dominating at small τ and the waning alignment at large τ.

The exponents ν and γ also display local maxima, but at somewhat larger τ. Their saturation values are much higher than the respective critical exponents in all known universality classes, including the standard VM. To attribute the observed finite-size scaling to a critical point in the infinite-size limit according to the conventional scaling hypothesis [57] would require an extraordinarily sharp divergence of the correlation length and the susceptibility at criticality, which is approached extraordinarily slowly with increasing particle number N [see the solid lines in Figs. 1(a) and 1(b). As detailed in Sec. S1 of the Supplemental Material [40], we expect the observed scaling to hold whenever the density is approximately homogeneous, as it is the case for intermediate N. Then, also, the standard VM shows the truly critical scaling of its incompressible variant [16,37], while, for very large N, it exhibits large density fluctuations leading to a discontinuous phase transition with microphase separation.

Time correlation functions.—The time dependence of the CFs [Eq. (3)] for the delay VM at the transition, quantifying the temporal loss of orientational correlations [4,15], is strongly influenced by the delay. Figure 2(a) shows that the normalized CFs $\bar{C}(t) \equiv C(k^*,t)/C(k^*,0)$ acquire oscillations with period $(\tau + 1)$ and an amplitude increasing with τ. They reveal the transmission of orientational correlations over discrete time steps $\tau + 1$ and can be understood analytically by a spin wave theory that accounts for the delay [40]. In Fig. 2(d), we show that logarithms of CFs for $N = 2^n$, $n = 8, \ldots, 11$, and $\tau = 0$ collapse onto the master curve $-t/\tau_R$ upon rescaling time by the relaxation times τ_R obtained from Eq. (S14) in the Supplemental Material [40]. Figure 2(g) shows the corresponding increasingly negative time derivatives for $t \to 0$, indicating the exponential loss of correlation in the standard VM [15]. Due to the delay-induced superimposed oscillations, the initial slope of the CFs always steepens with increasing

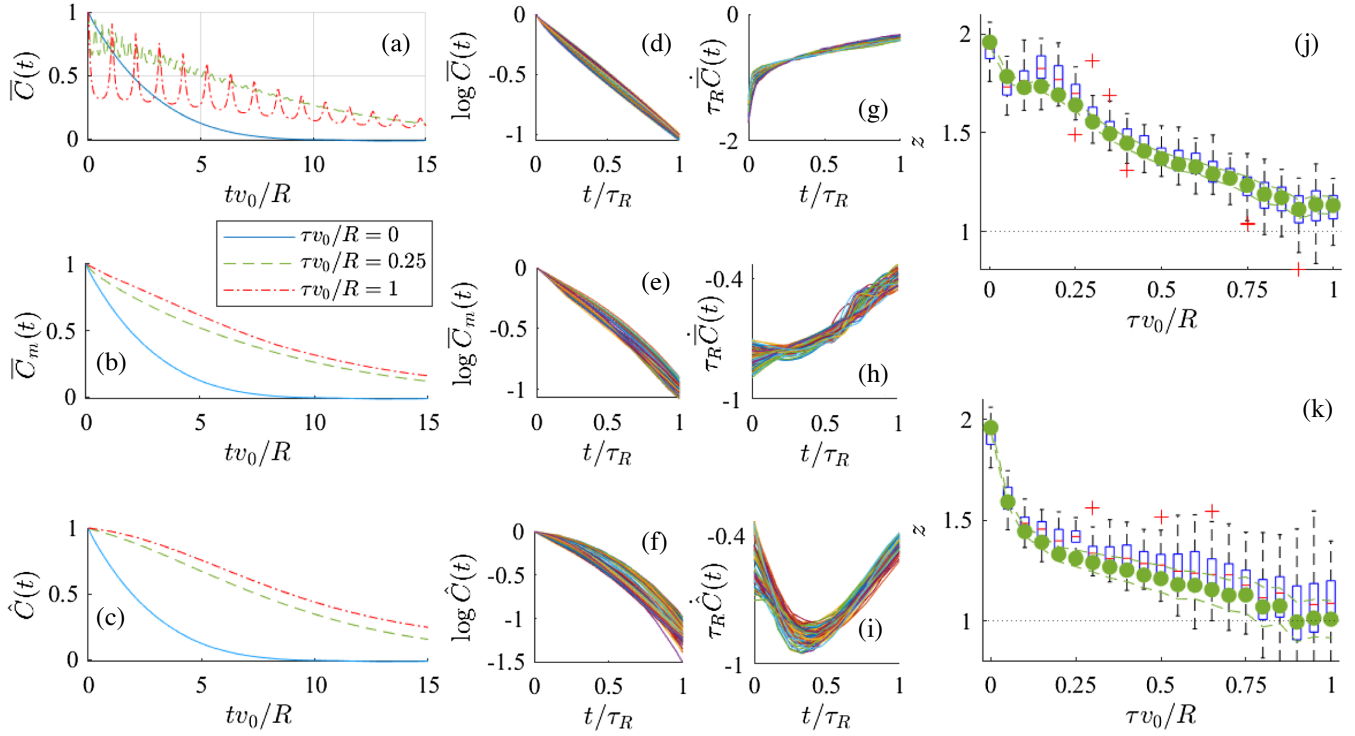

FIG. 2. Dynamical scaling of the orientational correlations at the susceptibility maximum displayed in Fig. 1. (a) Normalized time-correlation functions $\bar{C}(t)$ for delays $\tau = 0$, 5, 20 and $N = 2048$. (b) The upper envelopes $\bar{C}_m$ of the curves in (a). (c) The correlation functions $\hat{C}(t)$ calculated from trajectories (under)sampled with frequency $1/(\tau+1)$ for $N = 2048$. (d)–(f) The normalized CFs $\bar{C}$, $\bar{C}_m$, and $\hat{C}$ collapse upon measuring time in units of the relaxation time τ_R for $\tau = 0$ (d) and $\tau = 20$ (e) and (f) and system sizes $N = 2^n$, $n = 8, \ldots, 11$ (50 simulation runs for each system size). (g)–(i) The corresponding collapsed slopes. Box-plots [55] in (j) and (k) show the dynamical exponent z obtained from collapsing the CFs $\bar{C}_m$ and $\hat{C}$ by rescaling time as $t\xi^z$. Examples of the corresponding collapses are shown in Figs. S13 and S14 in the Supplemental Material [40]. The green circles are from linear fits to $\log \tau_R(N) = -z \log k^*(N)$ for all 50 datasets with 95% confidence intervals of the fits (dashed).

delay time τ. In contrast, the *overall* decay flattens with τ, as revealed by the upper envelopes $\bar{C}_m(t)$ of $\bar{C}(t)$, in Fig. 2(b). As intuitively expected, the delayed interactions thus tend to increase the memory in the VM. The data collapse of $\bar{C}_m(t/\tau_R)$ in Fig. 2 confirms the nonexponential relaxation, while its slope in Fig. 2(h) still increases for $t \to 0$ (see Sec. S5 in the Supplemental Material [40] for an approximate analytical result).

However, we note that the sampling rates used in practical measurements may not always be sufficient to resolve delay induced oscillations [40], which might moreover have a tendency to be washed out by a natural dispersion of the delay times. To account for undersampling, Fig. 2(c) shows normalized CFs $\hat{C}(t)$ calculated from particle positions that were (under-)sampled with frequency $1/(\tau+1)$, i.e., we calculated the corresponding velocities as $\mathbf{v}_i(t) = [\mathbf{r}_i(t) - \mathbf{r}_i(t-\tau-1)]/(\tau+1)$. In Fig. S10 of the Supplemental Material [40], we show that the undersampled CFs are independent of the sampling rate as long as it is comparable to or smaller than $1/\tau$. The resulting CFs are shown in Fig. 2(c). The exponential initial decay for the vanishing delay time $\tau = 0$ is seen to increasingly flatten with growing τ, as also corroborated by the data collapse in Fig. 2(f). For $v_0\tau/R \gtrsim 1/2$, the absolute slope $|\dot{\hat{C}}(t)|$ starts to decrease for $t \to 0$ as shown in Fig. 2(i) and in Figs. S7 and S9 in the Supplemental Material [40]. The undersampled delay VM yields qualitatively the same relaxation of orientational correlations as observed for natural swarms [15]. It thus provides an alternative explanation for the data, which were so far interpreted within the inertia spin model [58]. The dynamics induced by a discrete time delay appears to be more prone to developing oscillatory patterns, such as the ones illustrated in Fig. 2(a), though.

Dynamical scaling.—The dynamical scaling hypothesis [57] states that the relaxation time τ_R diverges with the correlation length as $\tau_R \sim \xi^z \sim (k^*)^{-z}$, at a critical point. Directly fitting the relation

$$\log \tau_R(N) = -z \log k^*(N) \tag{7}$$

for the relaxation times of $\bar{C}_m$ and $\hat{C}$ as functions of time delay τ yields the dynamical exponent z as depicted by circles in Figs. 2(j) and 2(k), respectively. The figures also show box plots [55] resulting from the best data collapse of CFs $\bar{C}_m$ and $\hat{C}$ using $(k^*)^{-z}$ with z as a free parameter in place

of the relaxation time τ_R, itself. The exponents z obtained from these two approaches nicely agree for each CF. While the values for z obtained from the two alternative CFs differ, they exhibit the same robust trend: a crossover from the overdamped equilibrium to the underdamped off-equilibrium signature [14,40], i.e., from $z \approx 2$ for $\tau = 0$ to about $z \approx 1.1$ for $\tau v_0/R \approx 1$ [59]. Our analysis thus suggests that increasing the delay time drives the system further from equilibrium as if one had effectively increased the particle speed v_0. Analytical arguments corroborate this, at least for large τ (Sec. S6 in the Supplemental Material [40]). Our results can therefore reconcile the standard VM predictions with the observations for natural swarms.

Conclusion.—We analyzed the VM with retarded interactions, as they are expected from natural delays between sensing and reaction. It provides an alternative to the rotational inertia hypothesis for reconciling the discrepancies in the dynamical scaling and relaxation between the standard VM and natural swarms [4,58]. While the navigation of insects and other flying species is certainly influenced both by inertia and time delay, our focus on delay could help to better understand their relation to feedback-driven robotic [35] or microparticle [24,25,60] swarms. Especially in the latter, current experimental techniques [26] allow inertial effects to be suppressed so that only the unavoidable time delay remains. While our analysis proves that the delay VM is compatible with finite-size scaling for the investigated system sizes, it raises many questions. Will larger systems exhibit a discontinuous transition with a phase separation, as in the standard VM? Will it mask the finite-size signatures of a continuous phase transition for practically relevant particle numbers? How does the phase diagram depend on the delay time? We hope to address some of these questions in the future.

We acknowledge funding through a DFG-GACR cooperation by the Deutsche Forschungsgemeinschaft (DFG Project No. 432421051) and by the Czech Science Foundation (GACR Project No. 20-02955J). V. H. was supported by the Humboldt Foundation. D. G. acknowledges funding by International Max Planck Research Schools (IMPRS). The time-correlation functions were computed at the GPU-Cluster Clara at the Scientific Computing Center in Leipzig. We are grateful to Lokrshi Dadhichi for his helpful remarks concerning the final manuscript and to Kiril Panayotov Blagoev for support during a preliminary stage of the project.

*viktor.holubec@mff.cuni.cz

[1] T. Mora and W. Bialek, Are biological systems poised at criticality?, J. Stat. Phys. **144**, 268 (2011).
[2] A.-L. Barabási and E. Bonabeau, Scale-free networks, Sci. Am. **288**, 60 (2003).
[3] M. A. Munoz, Colloquium: Criticality and dynamical scaling in living systems, Rev. Mod. Phys. **90**, 031001 (2018).
[4] A. Cavagna, I. Giardina, and T. S. Grigera, The physics of flocking: Correlation as a compass from experiments to theory, Phys. Rep. **728**, 1 (2018).
[5] M. Plischke and B. Bergersen, *Equilibrium Statistical Physics (3rd Edition)* (World Scientific Publishing Company, Singapore, 2006).
[6] P. Bak, C. Tang, and K. Wiesenfeld, Self-organized criticality, Phys. Rev. A **38**, 364 (1988).
[7] A. Clauset, C. R. Shalizi, and M. E. J. Newman, Power-law distributions in empirical data, SIAM Rev. **51**, 661 (2009).
[8] J. Jhawar, R. G. Morris, U. R. Amith-Kumar, M. Danny Raj, T. Rogers, H. Rajendran, and V. Guttal, Noise-induced schooling of fish, Nat. Phys. **16**, 488 (2020).
[9] G. Pruessner and H. J. Jensen, Broken scaling in the forest-fire model, Phys. Rev. E **65**, 056707 (2002).
[10] L. Palmieri and H. J. Jensen, The forest fire model: The subtleties of criticality and scale invariance, Front. Phys. **8**, 257 (2020).
[11] D. Martin, H. Chaté, C. Nardini, A. Solon, J. Tailleur, and F. Van Wijland, Fluctuation-Induced Phase Separation in Metric and Topological Models of Collective Motion, Phys. Rev. Lett. **126**, 148001 (2021).
[12] A. Cavagna, L. Di Carlo, I. Giardina, L. Grandinetti, T. S. Grigera, and G. Pisegna, Dynamical Renormalization Group Approach to the Collective Behavior of Swarms, Phys. Rev. Lett. **123**, 268001 (2019).
[13] T. Vicsek, A. Czirók, E. Ben-Jacob, I. Cohen, and O. Shochet, Novel Type of Phase Transition in a System of Self-Driven Particles, Phys. Rev. Lett. **75**, 1226 (1995).
[14] A. Cavagna, L. D. Carlo, I. Giardina, T. S. Grigera, S. Melillo, L. Parisi, G. Pisegna, and M. Scandolo, Natural swarms in 3.99 dimensions, arXiv:2107.04432.
[15] A. Cavagna, D. Conti, C. Creato, L. Del Castello, I. Giardina, T. S. Grigera, S. Melillo, L. Parisi, and M. Viale, Dynamic scaling in natural swarms, Nat. Phys. **13**, 914 (2017).
[16] A. Cavagna, L. Di Carlo, I. Giardina, T. S. Grigera, and G. Pisegna, Equilibrium to off-equilibrium crossover in homogeneous active matter, Phys. Rev. Research **3**, 013210 (2021).
[17] M. Nagy, Z. Ákos, D. Biro, and T. Vicsek, Hierarchical group dynamics in pigeon flocks, Nature (London) **464**, 890 (2010).
[18] A. Attanasi, A. Cavagna, L. Del Castello, I. Giardina, T. S. Grigera, A. Jelić, S. Melillo, L. Parisi, O. Pohl, E. Shen, and M. Viale, Information transfer and behavioural inertia in starling flocks, Nat. Phys. **10**, 691 (2014).
[19] D. Geiss, K. Kroy, and V. Holubec, Brownian molecules formed by delayed harmonic interactions, New J. Phys. **21**, 093014 (2019).
[20] G. Vásárhelyi, C. Virágh, G. Somorjai, N. Tarcai, T. Szörényi, T. Nepusz, and T. Vicsek, Outdoor flocking and formation flight with autonomous aerial robots, in *2014 IEEE/RSJ International Conference on Intelligent Robots and Systems* (IEEE, New York, 2014), pp. 3866–3873, 10.1109/IROS.2014.6943105.
[21] C. Virágh, G. Vásárhelyi, N. Tarcai, T. Szrényi, G. Somorjai, T. Nepusz, and T. Vicsek, Flocking algorithm for autonomous flying robots, Bioinspiration Biomimetics **9**, 025012 (2014).
[22] G. Vásárhelyi, C. Virágh, G. Somorjai, T. Nepusz, A. E. Eiben, and T. Vicsek, Optimized flocking of autonomous drones in confined environments, Sci. Rob. **3**, eaat3536 (2018).

[23] L. Davis, Modifications of the optimal velocity traffic model to include delay due to driver reaction time, Physica (Amsterdam) **319A**, 557 (2003).

[24] U. Khadka, V. Holubec, H. Yang, and F. Cichos, Active particles bound by information flows, Nat. Commun. **9**, 3864 (2018).

[25] S. Muiños-Landin, A. Fischer, V. Holubec, and F. Cichos, Reinforcement learning with artificial microswimmers, Sci. Rob. **6**, eabd9285 (2021).

[26] M. Fränzl, S. Muiños-Landin, V. Holubec, and F. Cichos, Fully steerable symmetric thermoplasmonic microswimmers, ACS Nano **15**, 3434 (2021).

[27] E. Forgoston and I. B. Schwartz, Delay-induced instabilities in self-propelling swarms, Phys. Rev. E **77**, 035203(R) (2008).

[28] R. Piwowarczyk, M. Selin, T. Ihle, and G. Volpe, Influence of sensorial delay on clustering and swarming, Phys. Rev. E **100**, 012607 (2019).

[29] S. A. M. Loos and S. H. L. Klapp, Heat flow due to time-delayed feedback, Sci. Rep. **9**, 2491 (2019).

[30] R. Erban, J. Hakovec, and Y. Sun, A cucker–smale model with noise and delay, SIAM J. Appl. Math. **76**, 1535 (2016).

[31] P. Romanczuk and G. Salbreux, Optimal chemotaxis in intermittent migration of animal cells, Phys. Rev. E **91**, 042720 (2015).

[32] A. Diz-Muñoz, P. Romanczuk, W. Yu, M. Bergert, K. Ivanovitch, G. Salbreux, C.-P. Heisenberg, and E. K. Paluch, Steering cell migration by alternating blebs and actin-rich protrusions, BMC Biol. **14**, 74 (2016).

[33] P. Bushev, D. Rotter, A. Wilson, F. Dubin, C. Becher, J. Eschner, R. Blatt, V. Steixner, P. Rabl, and P. Zoller, Feedback Cooling of a Single Trapped Ion, Phys. Rev. Lett. **96**, 043003 (2006).

[34] D. Goldwater, B. A. Stickler, L. Martinetz, T. E. Northup, K. Hornberger, and J. Millen, Levitated electromechanics: All-electrical cooling of charged nano- and micro-particles, Quantum Sci. Technol. **4**, 024003 (2019).

[35] M. Mijalkov, A. McDaniel, J. Wehr, and G. Volpe, Engineering Sensorial Delay to Control Phototaxis and Emergent Collective Behaviors, Phys. Rev. X **6**, 011008 (2016).

[36] F. Ginelli, The physics of the vicsek model, Eur. Phys. J. Spec. Top. **225**, 2099 (2016).

[37] L. Chen, J. Toner, and C. F. Lee, Critical phenomenon of the order–disorder transition in incompressible active fluids, New J. Phys. **17**, 042002 (2015).

[38] L. Chen, C. F. Lee, and J. Toner, Incompressible polar active fluids in the moving phase in dimensions $d > 2$, New J. Phys. **20**, 113035 (2018).

[39] C. Bechinger, R. Di Leonardo, H. Löwen, C. Reichhardt, G. Volpe, and G. Volpe, Active particles in complex and crowded environments, Rev. Mod. Phys. **88**, 045006 (2016).

[40] See Supplemental Material at http://link.aps.org/supplemental/10.1103/PhysRevLett.127.258001 containing additional Refs. [41–48], for additional numerical and theoretical results.

[41] D. R. J. Laming, *Information Theory of Choice-Reaction Times* (Academic Press, New York, 1968).

[42] P. C. Hohenberg and B. I. Halperin, Theory of dynamic critical phenomena, Rev. Mod. Phys. **49**, 435 (1977).

[43] A. T. Welford, *Reaction Times* (Academic Press, New York, 1980).

[44] R. C. Eaton, R. A. Bombardieri, and D. L. Meyer, The mauthner-initiated startle response in teleost fish, J. Exp. Biol. **66**, 65 (1977).

[45] R. C. Eaton, *Neural Mechanisms of Startle Behavior* (Springer Science & Business Media, 1984).

[46] P. Lenz and D. Hartline, Reaction times and force production during escape behavior of a calanoid copepod, undinula vulgaris, Mar. Biol. **133**, 249 (1999).

[47] H. Pomeroy and F. Heppner, Laboratory determination of startle reaction time of the starling (sturnus vulgaris), Anim. Behav. **25**, 720 (1977).

[48] T. D. Frank, P. J. Beek, and R. Friedrich, Fokker-planck perspective on stochastic delay systems: Exact solutions and data analysis of biological systems, Phys. Rev. E **68**, 021912 (2003).

[49] A. Attanasi, A. Cavagna, L. Del Castello, I. Giardina, S. Melillo, L. Parisi, O. Pohl, B. Rossaro, E. Shen, E. Silvestri, and M. Viale, Finite-Size Scaling as a Way to Probe Near-Criticality in Natural Swarms, Phys. Rev. Lett. **113**, 238102 (2014).

[50] M. E. Fisher and M. N. Barber, Scaling Theory for Finite-Size Effects in the Critical Region, Phys. Rev. Lett. **28**, 1516 (1972).

[51] S. Vogel, Flight in drosophila: I. Flight performance of tethered flies, J. Exp. Biol. **44**, 567 (1966).

[52] T. Beatus, J. M. Guckenheimer, and I. Cohen, Controlling roll perturbations in fruit flies, J. R. Soc. Interface **12**, 20150075 (2015).

[53] L. Ristroph, A. J. Bergou, G. Ristroph, K. Coumes, G. J. Berman, J. Guckenheimer, Z. J. Wang, and I. Cohen, Discovering the flight autostabilizer of fruit flies by inducing aerial stumbles, Proc. Natl. Acad. Sci. U.S.A. **107**, 4820 (2010).

[54] L. Ristroph, G. Ristroph, S. Morozova, A. J. Bergou, S. Chang, J. Guckenheimer, Z. J. Wang, and I. Cohen, Active and passive stabilization of body pitch in insect flight, J. R. Soc. Interface **10**, 20130237 (2013).

[55] Box-plot depicts statistics on data sets. The central mark indicates the median, and the bottom and top edges of the box indicate the 25th and 75th percentiles, respectively. The whiskers extend to the most extreme data points not considered outliers, and the outliers are plotted individually using the '+' symbol. (Taken from MATLAB documentation.).

[56] D. S. Cambui, A. S. de Arruda, and M. Godoy, Critical exponents of a self-propelled particles system, Physica (Amsterdam) **444A**, 582 (2016).

[57] B. Halperin and P. Hohenberg, Scaling laws for dynamic critical phenomena, Phys. Rev. **177**, 952 (1969).

[58] A. Cavagna, D. Conti, I. Giardina, T. S. Grigera, S. Melillo, and M. Viale, Spatio-temporal correlations in models of collective motion ruled by different dynamical laws, Phys. Biol. **13**, 065001 (2016).

[59] The saturation of $z(\tau)$ for large τ follows from that of $\xi(\tau)$ (implied by the saturation of the finite-size scaling parameters in Fig. 1) and $\tau_R(\tau)$ (Fig. S12 [40]).

[60] F. A. Lavergne, H. Wendehenne, T. Bäuerle, and C. Bechinger, Group formation and cohesion of active particles with visual perception–dependent motility, Science **364**, 70 (2019).